RSC Advances

PAPER

View Article Online
View Journal | View Issue



Cite this: *RSC Adv.*, 2015, **5**, 30192

# The effect of carbon black in carbon counter electrode for $CH_3NH_3PbI_3/TiO_2$ heterojunction solar cells

Heng Wang,* Xiaoyan Hu and Hongxia Chen

Received 23rd February 2015
Accepted 23rd March 2015

DOI: 10.1039/c5ra02325d

www.rsc.org/advances

Carbon counter electrodes (CCEs) based on pure flaky graphite, pure carbon black and graphite/carbon black composites were respectively applied in mesoscopic $CH_3NH_3PbI_3/TiO_2$ heterojunction solar cells. Crystallinity, conductivity and current–voltage characteristics were measured to study the influence of carbon black in the graphite/carbon black CEs on the perovskite crystal and the photovolatic performance of the devices. Results showed that the content of carbon black in the CCEs could significantly affect the crystallinity and uniformity of the perovskite crystal, leading to different photovolatic performance of the devices. The device with the optimized content of carbon black showed an efficiency of 7.08%, which was much higher than the efficiency of 2.75% obtained by the device based on graphite CE without carbon black.



## Introduction

In the past few years, lead halide perovskite solar cells have experienced the fastest increase in reported efficiencies ever achieved for any photovoltaic technology. In their early development, lead halide perovskite solar cells were fabricated with liquid electrolyte and showed low efficiencies.[1,2] In 2012, the first solid-state perovskite solar cell with an impressive efficiency of 9.7% was reported.[3] Soon after, much effort was devoted to developing solid-state perovskite solar cells.[4–7] Up to now, efficiencies over 15% have been obtained by many groups,[8–12] which make them a promising candidate of the next generation photovoltaic technology. However, the conventional counter electrodes (CEs) of perovskite solar cells are fabricated with noble metals under high vacuum conditions, which significantly increase the overall cost of the devices. Therefore, it is worth developing cost-effective CEs for perovskite solar cells. In 2013, Han's group reported using a carbon counter electrode (CCE) to fabricate a $CH_3NH_3PbI_3/TiO_2$ heterojunction solar cell, which showed a PCE of 6.64%.[13] In that work, $CH_3NH_3PbI_3$ was directly deposited in a $TiO_2/ZrO_2/C$ triple layer scaffold from $CH_3NH_3I$ and $PbI_2$ precursor solution. In 2014, a novel mixed-cation perovskite $(5\text{-AVA})_x(MA)_{1-x}PbI_3$ was filled into a $TiO_2/ZrO_2/C$ scaffold and an impressive PCE of 12.84% was achieved for perovskite solar cells based on this CCE.[14] Also perovskite solar cells based on CCEs using flaky graphite with different sizes were reported.[15] Usually, the CCEs are made by screen-printing or doctor-blading technique with graphite and carbon black as the main components.[16,17] Compared with conventional noble metal CEs, CCEs are more cost-effective due to their cheaper materials and easier processing methods. Moreover, because perovskite crystals form directly in a mesoscopic $TiO_2/ZrO_2/C$ scaffold for perovskite solar cells based on CCEs, the structure of the CCE films directly affect the particle size and uniformity of perovskite crystal,[13,15] which have great influence on the photovoltaic performance of perovskite solar cells.[18] Although CCE is a promising candidate for perovskite solar cells, few relevant studies on CCE for perovskite solar cells were reported. In this work, we studied the effect of carbon black in graphite/carbon black composite CEs on the photovolatic performance for mesoscopic $CH_3NH_3PbI_3/TiO_2$ heterojunction solar cells. The crystallinity and uniformity of perovskite crystals deposited on different CCEs based on flaky graphite, amorphous carbon black and graphite/carbon black composite were investigated respectively. For devices, current–voltage characteristics measurements were carried out to study the influence of the carbon black on the device performance. Results showed that carbon black in CCEs could weaken the crystallinity of $CH_3NH_3PbI_3$ crystal and improve the uniformity of the perovskite film, leading to increased photovolatic performance.

## Experimental

### Fabrication of carbon pastes

Graphite paste: 2 g flaky graphite powder (8000 mesh) and 0.2 g ethyl cellulose were added into 10 g terpineol. Carbon black paste: 2 g carbon black powder (30 nm) and 0.2 g ethyl cellulose were added into 10 g terpineol. Graphite/carbon black paste (20% content of carbon black): 1.6 g graphite powder, 0.4 g

*Department of New Energy, School of Physical Science and Electronic Technology, Yancheng Teachers University, Yancheng, Jiangsu, P.R. China, 224000. E-mail: wangheng8463@163.com; Tel: +86 0515 8825 8236*

carbon black powder and 0.2 g ethyl cellulose were added into 10 g terpineol. All the three mixture were followed by ball milling for 2 h.

### Fabrication of mesoscopic perovskite solar cells

The fluorine-doped $SnO_2$ substrates were etched with laser to form two detached electrode pattern before being cleaned ultrasonically cleaned with detergent, deionized water and ethanol respectively. After that the patterned substrates were coated with a 100 nm compact $TiO_2$ layer by aerosol spray pyrolysis at 450 °C. Then a 1 μm nanoporous $TiO_2$ layer was deposited on the compact $TiO_2$ layer by screen printing with a $TiO_2$ slurry and sintered at 500 °C for 30 min. And then, a $ZrO_2$ layer and a carbon film were printed on the top of the nanoporous $TiO_2$ layer successively, and sintered at 400 °C for 30 min, forming a porous $TiO_2/ZrO_2/C$ scaffold. The thicknesses of $ZrO_2$ layer and carbon layer were around 1 μm and 5 μm respectively. Finally, a 20 μl $CH_3NH_3PbI_3$ precursor (0.1 g $CH_3NH_3I$ and 0.29 g $PbI_2$ were mixed in 1 mL γ-butyrolactone) was dipped on the top of each $TiO_2/ZrO_2/C$ scaffold. Finally, the substrates were dried at 60 °C for 20 min in air under dark, resulting in the completion of devices.

### Characterization

The cross section of the devices and the top views of different CCEs were imaged by a field-emission scanning electron microscope (FE-SEM). The XRD spectra of the prepared films were tested by a X-ray diffraction system (85 PANalytical Empyrean, Cu Kα radiation; $\lambda = 1.5418$ Å). The square resistances of CCEs with different contents of carbon black were tested by four-probe measurement. Current–voltage characterization was performed using a Keithley 2400 source meter under simulated AM 1.5 sunlight illumination (100 mW $cm^{-2}$) provided by an Oriel solar simulator (Model 9119X, Newport Co.). The illuminated active area of photovoltaic measurements was 0.13 $cm^{-2}$. Incident photon-current conversion efficiency (IPCE) was recorded on a DC Power Meter (Model 2931-C, Newport Co.) under irradiation of a 300 W xenon lamp light source with a motorized monochromator (Oriel). The xenon lamp was powered by an Arc Lamp Power Supply (Model69920, Newport Co.).

## Results and discussion

### Structure of $TiO_2/CH_3NH_3PbI_3$ heterojunction perovskite solar cells based on CCEs

Fig. 1a shows a schemed structure of a $TiO_2/CH_3NH_3PbI_3$ heterojunction perovskite solar cell based on CCE where nanoporous $TiO_2$ layer, $ZrO_2$ insulating layer and carbon layer were screen-printed on FTO/compact $TiO_2$ substrate layer by layer. $CH_3NH_3PbI_3$ was filled in the pores of $TiO_2/ZrO_2/C$ triple layer films by one-step solution method from $PbI_2$ and $CH_3NH_3I$ precursor. Fig. 1b shows the energy levels of $TiO_2$, $CH_3NH_3PbI_3$ and C respectively. Fig. 2a and b show the SEM cross section of a $TiO_2/CH_3NH_3PbI_3$ heterojunction perovskite solar cell and its high magnification $TiO_2/CH_3NH_3PbI_3$ layer, respectively. In Fig. 2a, it is clear that 1 μm $TiO_2$ layer, 1 μm $ZrO_2$ layer and 5 μm

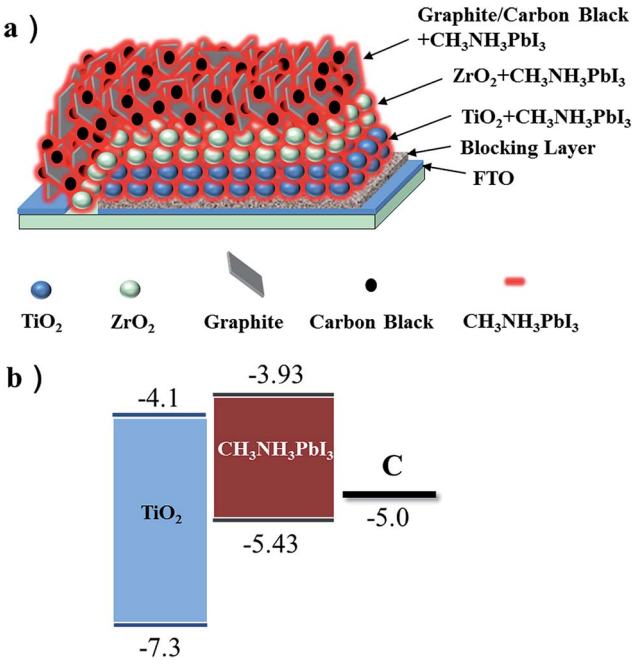


Fig. 1 (a) A schemed structure of $CH_3NH_3PbI_3/TiO_2$ heterojunction solar cells based on CCE. (b) The corresponding energy levels of $TiO_2$, $CH_3NH_3PbI_3$ and carbon.

carbon layer are ordinarily deposited on the surface of FTO glass. From Fig. 2b, we could see that $CH_3NH_3PbI_3$ is filled in the pores of nanoporous $TiO_2$, and the bright region and dark region represent $TiO_2$ and $CH_3NH_3PbI_3$ respectively.

### Characterization of $CH_3NH_3PbI_3$ crystal deposited on different carbon films

We deposited three different carbon films on glasses by screen-printing with graphite paste, carbon black paste, and graphite/

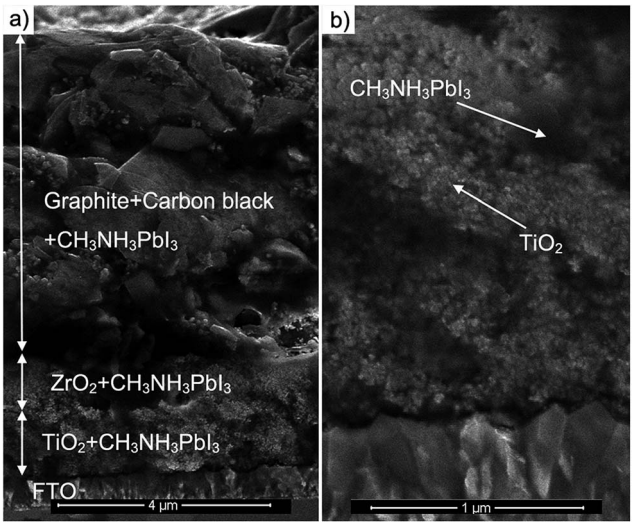


Fig. 2 (a) The SEM cross section of a $TiO_2/CH_3NH_3PbI_3$ heterojunction perovskite solar cell based on CCE. (b) The high magnification $TiO_2/CH_3NH_3PbI_3$ layer.

carbon black paste respectively. After sintering at 400 °C for 30 min, the thicknesses of the films were around 5 μm. Then a precursor solution of $PbI_2$ and $CH_3NH_3I$ was dropped on each of the three different carbon films and dried at 60 °C to forming $CH_3NH_3PbI_3$ perovskite crystal. Fig. 3a–c show the SEM sections of the three carbon films respectively. The particle sizes of flaky graphite distribute from hundreds of nanometres to several microns (Fig. 3a) and the particle size of carbon black is tens of nanometres (Fig. 3c). Fig. 3d–f show the SEM section of $CH_3NH_3PbI_3$ perovskite crystals deposited on the three different carbon films respectively. From Fig. 3d we could see that $CH_3NH_3PbI_3$ deposited on graphite film show inhomogeneous morphology and show wide crystallite sizes distribution from hundreds of nanometres to several microns. From Fig. 3e and f we could see that $CH_3NH_3PbI_3$ deposited on carbon films containing carbon black show uniform and compact crystalline film, and no large crystallite was observed. This could be attributed that the nanoporous structure of carbon black limited the growth of $CH_3NH_3PbI_3$ crystal.

In order to understand the effect of carbon black in CCEs on the crystallinity of $CH_3NH_3PbI_3$ perovskite crystal, we carried out X-ray diffraction (XRD) patterns of $CH_3NH_3PbI_3$ deposited on the three carbon films and on bare glass, which were compared in Fig. 4. The diffraction peaks near 27° and 55° are the main characteristic peaks of flaky graphite. The diffraction peaks at the lattice planes of (110), (220), (310), (224) and (314) are the main characteristic peaks of $CH_3NH_3PbI_3$ deposited on bare glass. Among the three carbon films, $CH_3NH_3PbI_3$ deposited on carbon black film show the weakest diffraction intensities at most of the main characteristic peaks. And the diffraction intensities of $CH_3NH_3PbI_3$ on carbon black film are even weaker than that on bare glass. This could be attributed that the nanoporous structure of carbon black could limit the growth of $PbI_2$ and $CH_3NH_3PbI_3$ successively, resulting in decreased crystallinity. And among the three carbon films, $CH_3NH_3PbI_3$ deposited on graphite film show the strongest diffraction intensity at most of the main characteristic peaks. This is consistent with the large particle size of $CH_3NH_3PbI_3$ on graphite film which could be seen from Fig. 3d. Compared with $CH_3NH_3PbI_3$ on graphite film, $CH_3NH_3PbI_3$ on graphite/carbon black film exhibit decreased diffraction intensity at most of the characteristic peaks except the peak of (100). The decreased diffraction intensity of $CH_3NH_3PbI_3$ for graphite/carbon black film could be due to the limitation effect of the nanoporous structure of carbon black.

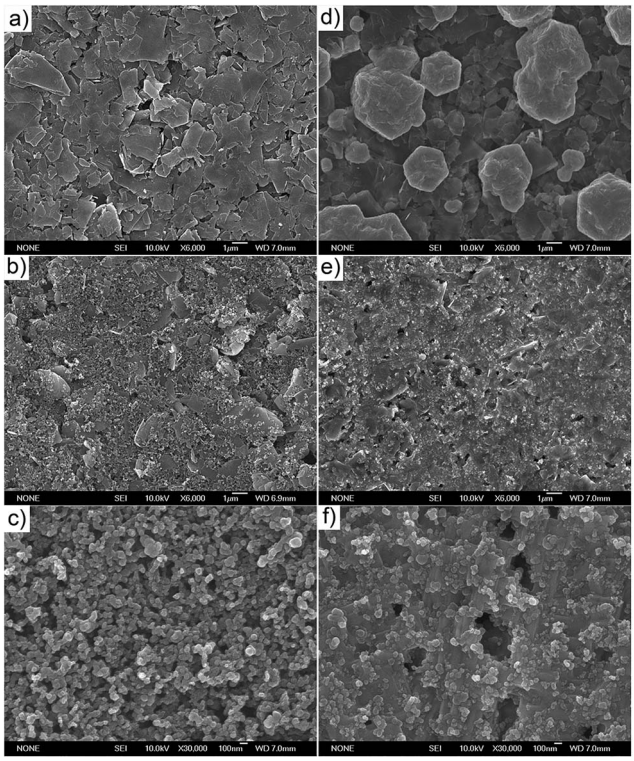


Fig. 3 (a–c) Top view SEM images of bare CCEs based on graphite, graphite/carbon black and carbon black, respectively. (d–f) Top view SEM images of the three corresponding CCEs infiltrated with $CH_3NH_3PbI_3$ from precursor solution of $PbI_2$ and $CH_3NH_3I$.

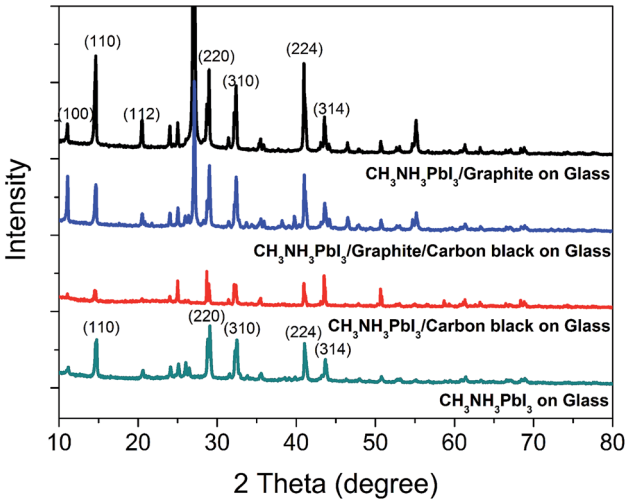


Fig. 4 XRD patterns of $CH_3NH_3PbI_3$ deposited on three carbon CCEs based on graphite, graphite/carbon black and carbon black and $CH_3NH_3PbI_3$ deposited on bare glass is also displayed.

## Characterization of devices with different contents of carbon black in CCEs

The photocurrent density–voltage curves of $TiO_2/CH_3NH_3PbI_3/C$ devices with different contents of carbon black in CCEs are displayed in Fig. 5. The photovoltaic performance of devices with different contents of carbon black in CCEs are displayed in Table 1. The device based on pure graphite CE showed poor photovoltaic characteristics with open-circuit voltage ($V_{oc}$), short-circuit current density ($J_{sc}$), fill factor (FF) and power conversion efficiency (PCE) of 753 mV, 6.96 mA $cm^{-2}$, 0.53 and 2.75% respectively. The photovoltaic performances of devices were improved with the increase of carbon black contents in CCEs. When 10% content of carbon black was induced into CCEs, $V_{oc}$, $J_{sc}$ and PCE of the device were increased to 844 mV, 12.45 mA $cm^{-2}$ and 5.54% respectively. The best performance of the devices was obtained when the contents of carbon black was

 

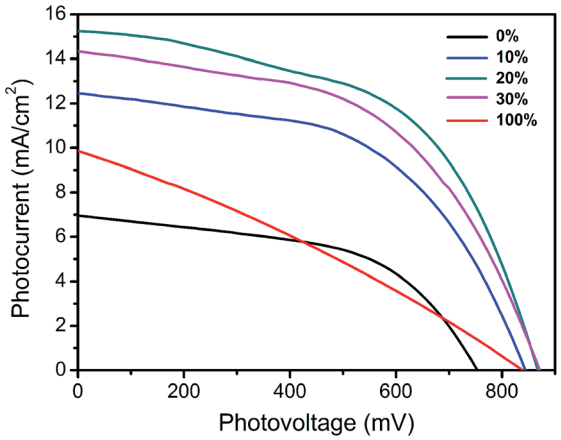


Fig. 5 Photocurrent density–voltage curves of devices based on CCEs with different contents of carbon black under standard simulated AM 1.5 illumination of 1000 W m$^{-2}$.

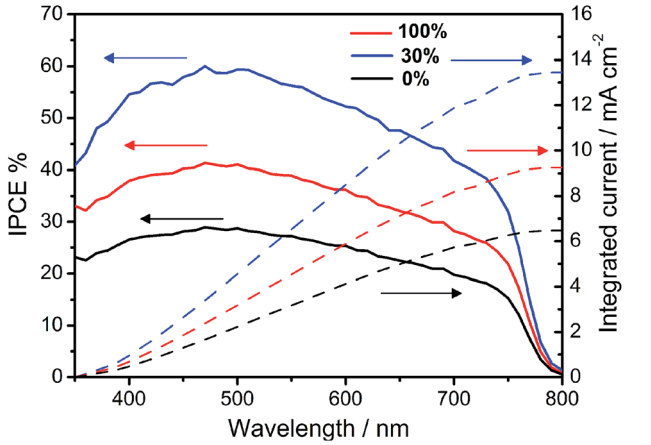


Fig. 6 IPCE curves for devices based on CEs with 0% (black curve), 30% (blue curve) and 100% (red curve) contents of carbon black respectively. The integrated photocurrents calculated from the overlap integral of the IPCE spectra with the AM 1.5 solar emission.

Table 1 Photovoltaic performance of $TiO_2$/$CH_3NH_3PbI_3$/C devices with different contents of carbon black in CCEs under AM 1.5 conditions 100 mW cm$^{-2}$. The thickness of $TiO_2$, $ZrO_2$ and C films are ~1 μm, ~1 μm and ~5 μm respectively

| Contents (wt%) | $J_{sc}$/mA cm$^{-2}$ | $V_{oc}$/mV | FF | PCE (%) |
|---|---|---|---|---|
| 0% | 6.96 | 753 | 0.53 | 2.75 |
| 10% | 12.45 | 844 | 0.53 | 5.54 |
| 20% | 15.24 | 867 | 0.54 | 7.08 |
| 30% | 14.34 | 871 | 0.52 | 6.44 |
| 100% | 9.85 | 839 | 0.30 | 2.46 |

20% in CCEs, which exhibited a $V_{oc}$ of 867 mV, a $J_{sc}$ of 15.24 mA cm$^{-2}$ and an efficiency of 7.08%. However, when the contents of carbon black were further increased, the efficiencies of devices were decreased. The device with 30% content of carbon black showed a $V_{oc}$ of 871 mV, a $J_{sc}$ of 14.34 mA cm$^{-2}$, a FF of 0.52 and a PCE of 6.44%. And the device based on pure carbon black CE obtained a $V_{oc}$ of 839 mV, a $J_{sc}$ of 9.85 mA cm$^{-2}$ and a FF of 0.30, resulting in a poor efficiency of 2.46%. The improved performances for devices with low contents of carbon black in CCEs could be attributed to the improved uniformity of perovskite film, which was subsequently critical to efficient perovskite solar cells.[11] The poor performance for device with 100% content of carbon black in CCEs could be due to the poor conductivity of pure carbon black CEs since poor conductivity of CEs could directly lead to low FF value for the device.[19]

In order to investigate the effect of carbon black on $J_{sc}$ of the devices, we measured the IPCE curves of the devices. Fig. 6 shows IPCE curves for devices based on CEs with 0%, 30% and 100% contents of carbon black respectively. The integrated photocurrents calculated from the overlap integral of the IPCE spectra with the AM 1.5 solar emission are also shown in Fig. 6. The integrated photocurrents for devices based on CEs with 0%, 30% and 100% contents of carbon black are 6.48 mA cm$^{-2}$, 13.45 mA cm$^{-2}$ and 9.26 mA cm$^{-2}$ respectively. These results are close to the $J_{sc}$ of 6.96 mA cm$^{-2}$, 14.34 mA cm$^{-2}$ and 9.85 mA cm$^{-2}$ obtained by the initial $I$–$V$ testing respectively. In order to further understand the effect of carbon black, we tested the square resistance of 5 μm thick CCEs with different content of carbon black, which are represented in Table 2. It is clear that the square resistance of CCEs increase gradually with the content of carbon black was increased. The decreased $J_{sc}$ and FF for devices with high contents of carbon black in CCEs is probably due to the high square resistance of CCEs, which subsequently results in decreased charge collection efficiency.

Table 2 Square resistance of 5 μm thick CCEs with different contents of carbon black in CCEs

| | 0% | 10% | 20% | 30% | 100% |
|---|---|---|---|---|---|
| $R_{sq}$ (Ω) | 40.4 | 76.4 | 114.4 | 164.4 | 864.4 |

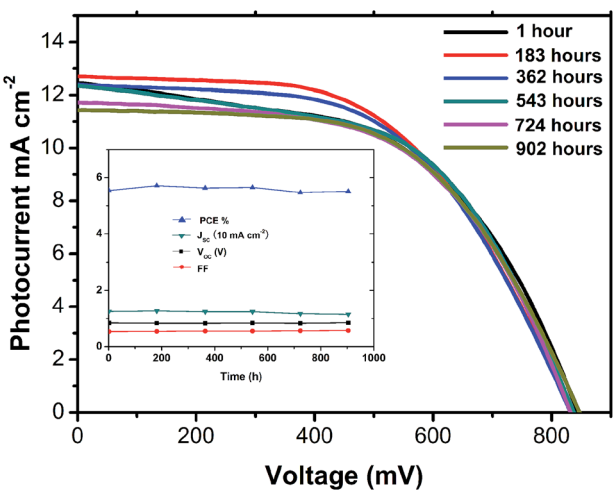


Fig. 7 Long term stability at room temperature in the dark. Inset: the changing characters of the device in 902 h after been fabricated.

The long-term stability in the dark of devices based on graphite/carbon black CE with the initial efficiency of 5.52% was tested under conditions stored in air atmosphere at room temperature without encapsulation and presented in Fig. 7. It could be found that after more than 900 hours, although the $J_{sc}$ decreased slightly, the PCE still remained over 5.5%.These results indicate the superior stability of $CH_3NH_3PbI_3/TiO_2$ heterojunction solar cells based on CCEs.

## Conclusions

In conclusion, as one of the main components in CCEs, carbon black has significant influence not only on the conductivity of CCEs but also on the crystallinity and uniformity of $CH_3NH_3PbI_3$ deposited on CCEs, which will eventually affect the photovoltaic performance of devices. Devices based on graphite/carbon black CEs with different contents of carbon black were made to study the influence of carbon black. Results show that carbon black could decrease the crystallinity of $CH_3NH_3PbI_3$ crystallites and improve uniformity of $CH_3NH_3PbI_3$ film on CCEs, leading to improved photovoltaic performance for mesoscopic $CH_3NH_3PbI_3/TiO_2$ heterojunction solar cells.

## Acknowledgements

The authors acknowledge the financial support from National Natural Science Foundation of China (no. 11404279). We thank the experiment center of Yancheng Teachers University for field emission scanning electron microscopy (FE-SEM) testing. We thank Michael Grätzel Center for Mesoscopic Solar Cells of Wuhan National Laboratory for Optoelectronics for current–voltage characterization and IPCE curves testing.

## Notes and references

1 A. Kojima, K. Teshima, Y. Shirai and T. Miyasaka, *J. Am. Chem. Soc.*, 2009, **131**, 6050.
2 J. H. Im, C. R. Lee, J. W. Lee, S. W. Park and N. G. Park, *Nanoscale*, 2011, **3**, 4088.
3 H.-S. Kim, C.-R. Lee, J.-H. Im, K.-B. Lee, T. Moehl, A. Marchioro, S.-J. Moon, R. Humphry-Baker, J.-H. Yum, J. E. Moser, M. Grätzel and N.-G. Park, *Sci. Rep.*, 2012, **2**, 591.
4 M. M. Lee, J. Teuscher, T. Miyasaka, T. N. Murakami and H. J. Snaith, *Science*, 2012, **338**, 643.
5 H. Chen, X. Pan, W. Liu, M. Cai, D. Kou, Z. Huo, X. Fang and S. Dai, *Chem. Commun.*, 2013, **49**, 7277.
6 B. Cai, Y. Xing, Z. Yang, W.-H. Zhang and J. Qiu, *Energy Environ. Sci.*, 2013, **6**, 1480.
7 W. A. Laban and L. Etgar, *Energy Environ. Sci.*, 2013, **6**, 3249.
8 Z. Xiao, C. Bi, Y. Shao, Q. Dong, Q. Wang, Y. Yuan, C. Wang, Y. Gao and J. Huang, *Energy Environ. Sci.*, 2014, **7**, 2619.
9 N. J. Jeon, J. H. Noh, Y. C. Kim, W. S. Yang, S. Ryu and S. I. Seok, *Nat. Mater.*, 2014, **13**, 897.
10 H. Zhou, Q. Chen, G. Li, S. Luo, T.-b. Song, H.-S. Duan, Z. Hong, J. You, Y. Liu and Y. Yang, *Science*, 2014, **345**, 542.
11 M. Liu, M. B. Johnston and H. J. Snaith, *Nature*, 2013, **501**, 395.
12 J. Burschka, N. Pellet, S.-J. Moon, R. Humphry-Baker, P. Gao, M. K. Nazeeruddin and M. Grätzel, *Nature*, 2013, **499**, 316.
13 Z. Ku, Y. Rong, M. Xu, T. Liu and H. Han, *Sci. Rep.*, 2013, **3**, 3132.
14 A. Mei, X. Li, L. Liu, Z. Ku, T. Liu, Y. Rong, M. Xu, M. Hu, J. Chen, Y. Yang, M. Grätzel and H. Han, *Science*, 2014, **345**, 295.
15 L. Zhang, T. Liu, L. Liu, M. Hu, Y. Yang, A. Mei and H. Han, *J. Mater. Chem. A*, 2015, DOI: 10.1039/c4ta04647a.
16 Z. Huang, X. Liu, K. Li, D. Li, Y. Luo, H. Li, W. Song, L. Chen and Q. Meng, *Electrochem. Commun.*, 2007, **9**, 596.
17 A. Kay and M. Grätzel, *Sol. Energy Mater. Sol. Cells*, 1996, **44**, 99.
18 Y. Wu, A. Islama, X. Yang, C. Qin, J. Liu, K. Zhang, W. Peng and L. Han, *Energy Environ. Sci.*, 2014, **7**, 2934.
19 G. Liu, H. Wang, X. Li, Y. Rong, Z. Ku, M. Xu, L. Liu, M. Hu, Y. Yang, P. Xiang, T. Shu and H. Han, *Electrochim. Acta*, 2012, **69**, 334.

 